Electrical Power and Energy Systems 163 (2024) 110317

Contents lists available at ScienceDirect

International Journal of Electrical Power and Energy Systems

journal homepage: www.elsevier.com/locate/ijepes

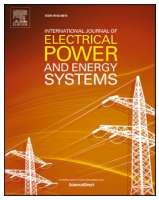

Enhancing voltage stability of grid forming power converters based on model predictive controller

Qudrat Ullah [a,*], Enio Costa Resende [a,b], Luiz Carlos Gomes Freitas [b], Hannu Laaksonen [a], Marcelo Godoy Simões [a]

[a] School of Technology and Innovations, University of Vaasa, Vaasa 65100, Finland
[b] Faculty of Electrical Engineering, Federal University of Uberlandia, Uberlandia 38.400-902, Brazil

ARTICLE INFO

Keywords:
Voltage source inverters
Grid forming converters
Standalone operation
Model predictive control
AC microgrids

ABSTRACT

This research article proposes an advanced control strategy based on a finite control set model predictive controller (FCS-MPC) for parallel-connected voltage source inverters (VSIs) for standalone operation of AC microgrids (MGs). The AC MGs may be consisted of two or more parallel connected VSIs connected and have ability to regulate the output line to line voltages at the point of common coupling (PCC) sustaining the local power demand. It is possible to attain these functionalities using traditional and linear control approaches, but there exist several challenges like sensitivity problems associated to parametric and non-parametric variations and they are unable to handle with existing constraints in system and resulting in slow dynamic response. An imperative feature of this research study is that proportional integral (PI) as well as proportional resonant (PR) controller based VSI was designed, studied and its performance was compared with FCS-MPC based VSI. The proposed FCS-MPC-based scheme handles several challenges effectually by confirming a stable and robust operation for Gridforming (GFM) inverters of AC MGs. In this scheme, the voltage reference over the predictive horizon is tracked by formulating a cost function (CF) and droop control is used to attain power sharing among distributed generations (DGs). The operation of standalone AC MG is authenticated by extensive simulations in MATLAB/Simulink environment, demonstrating that the FCS-MPC strategy shows quick dynamic response, improved power quality as well as enhanced voltage stability. The simulation results also reveal that total harmonic distortion (THD) of output line to line voltages is 0.86% for linear loads and 0.98 % for nonlinear loads, verifying that the THD level is primarily in the acceptable range defined by the IEC as well as IEEE standards, highlighting the AC MG system's compliance with international standards.

1. Introduction

Nowadays, the entire world is directed towards the use of Renewable Energy Resources (RERs). Different types of renewable energy exist in each country across the world. There has been immense progress in the field of green energy as well as the power harvesting approaches from RERs in the previous decade [1]. It is assessed that there is still a significant possibility of progress remaining in the field of RERs in the near future [2]. It has been noted recently that the world's energy systems are preparing to "decentralize, decarbonize, and democratize," in many cases from the bottom up [3] because there is a constantly increasing demand for electrical power energy due to the rise in population and industrial growth [4]. The power production industry suffers various problems, like the continuous energy supply at lower costs. The majority of electrical energy is still produced from non-renewable energy resources. So, fossil fuels are being depleted rapidly. Lately, strategies, for example, feed-in tariffs, along with the prevention of global warming to encourage the use of renewable energy systems, have been applied [5]. Thus, energy production approaches which practice sustainable energy have captivated momentous attention [6]. Power electronics converters significantly expand power utilization from RERs or DGs through advanced MGs to minimize electricity expenditures besides reducing dependency on power from utility grids.

The MGs are an evolving perspective in the contemporary era, directing to advance the power quality distributed to the neighbourhood loads and guaranteeing an enhanced and trustworthy power supply in several progressive contexts. The MGs face severe challenges of frequency and voltage control due to the increased inverter based power generation [7]. So, MGs have a substantial importance in realizing the

* Corresponding author.
E-mail address: qudrat.ullah@uwasa.fi (Q. Ullah).

https://doi.org/10.1016/j.ijepes.2024.110317
Received 18 January 2024; Received in revised form 3 September 2024; Accepted 15 October 2024
Available online 5 November 2024

Nomenclature

FCS-MPC	Finite control set model predictive controller
VSIs	Voltage source inverters
MGs	Microgrids
CF	Cost function
DGs	Distributed generations
THD	Total harmonic distortion
RERs	Renewable Energy Resources
GFM	Grid-forming
PWM	Pulse width modulator
DERs	Distributed energy resources
P	Active power
Q	Reactive power
V	Voltage
f	Frequency
ω	Angular frequency
I_L	Current before the filter inductor
V_{cap}	Voltage across the capacitor/output voltage
I_{out}	Output current
r_L	Equivalent series resistance of inductor
C_f	Filter capacitance
L_f	Filter inductance
V_x	Input voltage from inverter
V_{in}	DC link voltage
P_{cal}	Measured active power for droop control
Q_{cal}	Measured reactive power for droop control
V*	Reference voltage
OSS	Optimal switching sequence
OSV	Optimal switching vector
f *	Reference frequency
S_{opt}	Optimal switching states
P_c	Change in active power
Q_c	Change in reactive power
T_{samp}	Sampling time
ω*	Reference angular frequency
V_n	Nominal voltage
ω_n	Nominal frequency
S_a, S_b, S_c,	Legs of the three-phase VSI
V_{in}	DC link voltage
P*	Reference for active power
Q*	Reference for reactive power
LPF	Low pass filter
LV	Low voltage

larger penetration of RERs [8], and it is possible to configure these MGs in islanded or grid-connected operations depending on the economic and physical features of the region [9]. MGs can be classified into distinct categories. These categories are generally dependent on control strategy, distribution, means of operation, and generation sources. Centralized, decentralized, alongwith distributed mechanisms are based on the control methodologies of MGs. A central controller is required for a centralized control mechanism and is linked to generation sources and loads with the help of communication systems. This controller acquires as well as evaluates data from all neighbouring controllers to find optimum solutions without reiterations [10]. It can be considered a more straightforward controller because it is able to control power deliverance from a defined point. Still, it has many challenges associated with latency, communication protocols, scalability, and the single point of failure. Also, some critical issues related to the centralized control mechanism for MGs in distant sites make this scheme unrealistic and very expensive [11]. Since the central controller is not present in a decentralized control scheme, several control units possess separate control instructions [12]. A comprehensive comparative analysis between AC and DC MGs is provided [13,14]. In modern energy networks, renewable power-based DGs are more prevalent near the consumer premises to meet the load demand [15,16,1].

From the above discussion, it is clear that the developed and designed MGs should be simply well-balanced and manageable [17,18]. These MGs can be classified as DC and AC MGs. The best application of DC MGs is at what time the generation sources are DC, e.g., solar panels, the electrical appliances, and loads to be connected are fundamentally DC, and the network used for interconnecting them should be DC as well [19]. The DC MGs are more attractive regarding control strategies and efficiency, but an AC power supply is needed for the most traditional loads [20]. Power electronic converters, which act as an interface between RERs and an AC bus in the AC MGs, are necessary to handle the power flow. Among these power electronic converters, voltage source inverters (VSIs) are of pivotal importance in AC MGs because of power quality enhancement, power flow control, grid integration flexibility, modularity, scalability, quick dynamic response, and islanding detection and control. Nowadays, a considerable amount of power is obtained from uncontrollable natural resources having different dynamic aspects as well as steady-state features of DGs; thus, MGs possess numerous features and benefits that distinguish them from traditional power infrastructures, for example, enhanced flexibility and reliability [21,22], utilizing and capturing of energy produced as a by-product during the power generation procedure in DGs from coupled MGs, and use of these DGs apart from disrupting the main system proficiency [23].

The AC MGs can coordinate and control multiple VSIs simultaneously, providing greater flexibility than individual RERs working individually. Due to the lack of inertia and constant voltage source, the control mechanism of parallel connected VSIs forming an AC MG becomes challenging. These VSIs can be categorized as grid-feeding, grid-supporting, and grid-forming (GFM) converters based on their functionality. The grid-supporting and grid-feeding VSIs universally operate in grid-connected operational mode. In these operating modes, they actively interact with the grid and are synchronized with the power grids for the purpose of either providing stability and support (grid-supporting) by regulating frequency, voltage, and power control-related functionalities or supplying power to the utility grid (grid-feeding). To ensure the most effective control mechanism for these VSIs, exploring the reliable control schemes of the AC MGs is necessary. In grid-connected MGs operations, PQ control is usually deployed to give and take reactive and active power between the utility grids and MGs by maintaining and synchronizing frequency and voltage levels in an acceptable range [24–26]. The V/f control is generally used in islanded/stand-alone operating modes. This control strategy is sensitive to temperature drifts, crystal differences, and ageing, causes voltage and frequency deviations, and is usually not preferred for parallel-connected inverters [27]. In stand-alone operation, this strategy ensures frequency regulation by controlling output active power, while voltage is regulated by controlling output reactive power [28–30]. Several control schemes have been proposed in the literature regarding MG's different functionalities and operating conditions. Among them, the hierarchical control scheme is the most stated one for control of MGs, wherever several existing control strategies can be observed in its context [30]. Primary, secondary, as well as tertiary-level control schemes are considered essential components of the most typical hierarchical control structure [31–34]. It is usually necessary to accomplish the operation of the parallel connected VSIs in a decentralized manner [35], where no external communication is required. For this purpose, the conventional droop control scheme and its several advanced modified forms are used [36–40]. In these schemes, the droop controller generates the voltage reference, which operates in the outer control loop and modified droop

is introduced in [41]. In addition to this outer loop, an inner control loop receives this voltage reference. This inner loop usually consists of a voltage regulation loop and virtual impedance [42]. The fixed output impedance value is established using virtual impedance, thereby enabling reactive and active power control decoupling [43]. In contrast, voltage regulation is achieved by controlling the output voltage at the filter following the specified reference value. The overall VSIs control schemes of AC MGs based on conventional ways are pulse width modulator (PWM) techniques and hierarchically systematized linear loops [39,44,45]. This method has some practical limitations; for instance, the bandwidth of the outer loop is intentionally set with a smaller magnitude than the inner loop, resulting in a slower transient response [46].

Besides this, the control parameters of the system have a critical role in the overall system's stability. Therefore, careful considerations are necessary to tune these control parameters [47]. Ultimately, the usual hypothesis in the majority of research publications is based on a standard sampling value of all the VSIs by default, so practically achieving this condition demands the synchronization of several operating VSIs as well as fundamentally regulated like a single converter, resulting in an apparent conflict for the enthusiasm of the decentralized control approach [48]. Therefore, MGs should be controlled intelligently to ensure smooth performance and control scheme of VSIs of AC MGs should present a quick dynamic response for input voltage variations and load transitions. Based on quick dynamic performance, a fascinating approach to realize precise tracking of the voltage reference is using MPC for GFM VSIs. Some of the commonly used control schemes of MPC are optimal switching sequence (OSS) based MPC, optimal switching vector (OSV) based MPC, generalized MPC, and explicit MPC. The OSS-MPC can handle both non-linear and linear problems, but it has been known as the one which consumes the most time to computational efforts. The OSS-MPC does not need a modulator and it works under a constant switching frequency. The cost-function is minimized online with allowed constraints and possess short prediction horizon and algorithm complexities are intuitive [49,50,51]. While generalized MPC also works under a constant switching frequency and deals with unconstrained linear problems with minimum computational efforts. But it needs a modulator and typically practices complex algorithms complexity as compared to other control schemes as well as it is distinguished by long prediction horizon [52,53]. The explicit MPC has low computational cost and is mostly used for nonlinear constrained problems and modulator is also required for its operation while cost function is minimized offline and possesses complex algorithm and long prediction horizon [54,55,56]. The OSV-MPC based control scheme can solve both linear and nonlinear problems, and has a high computational complexity. Like OSS-MPC, it also does not need modulator and also usually has short prediction horizon and possesses intuitive algorithm [57,58,59].

The FCS-MPC which belongs to OSV-MPC is implemented in this study and it uses a discrete set of voltage vectors. The VSIs then use these voltage vectors to switch their output. To conclude, an overview of dominated control schemes with pros and cons for VSIs and MGs is provided in Table 1. To organize and show the effectiveness of the proposed solution, the remaining sections of this paper are presented in the following sequence. The section 1 encapsulates the introduction, including the background, literature review, and dominant control strategies of VSIs for MGs. The section 2 provides the system description. The section 2.1 succincts the droop control strategy for power sharing between DGs. The section 3 summarizes the mathematical representation of Distributed Energy Resources (DERs). The VSI is modeled in section 3.1. The section 3.2 system dynamics and state space representation. The cost function is formulated in section 3.3. The section 3.4 discusses the theoretical analysis of the proposed scheme. The section 4 provides results and discussion for the proposed control mechanism. The analysis for VSIs for AC MG is listed in section 4.1. The detailed simulations for VSI based on PR controller are provided in section 4.2. The analysis for VSI based MPC is provided in section 4.3, while characterization of load transitions for individual inverter are given in section 4.4. Moreover, comparison of performance for PI, PR and MPC based VSI is demonstrated in section 4.5. Similarly, analysis of standalone AC MG under steady-state conditions is provided in section 4.6 and characterization of load transitions for AC MG is detailed in section 4.7. Finally, section 5 provides the conclusion of this study.

2. System description

The circuit diagram of VSI used for AC MG is depicted in Fig. 1. The purpose of these VSIs is to operate like an ideal primary AC voltage source. In the stand-alone operation of AC MGs, these VSIs establish a reference voltage for the load system of AC MGs without relying on the external utility grid connection. The current before the filter inductor (I_L), the voltage across the capacitor (V_{cap}), and the phase to phase output current (I_{ou}) of the load are measured initially; then, these measurements are converted into a two-phase orthogonal reference frame. The system achieves smooth output voltages and handles load transitions with the help of MPC and droop control.

For the challenging multiple-objective control problem of multilevel inverters (MLIs), MPC has shown significant potential to control it [60]. Several modifications have been made over the past few years in MPC for MLI applications, including the reduction of computational workload, design of cost functions, modeling accuracy, and realization with a long forecast horizon. Thus, MPC is an effective control technique that employs an optimization-based control approach. It uses a dynamic process model for predicting the future behavior of the systems state variables as well as outputs. The problem of optimizing control objectives is formulated, with the inputs to the system acting as control variables. This problem is then resolved at different intervals within the prediction horizon by the predictive model, showing how the input sequences affect an objective function value. Finally, the system receives the initial input control action. It helps in controlling multiple variables regarding the power electronic switching devices as it deals with several challenges found in real world conditions related to voltage, current, frequency and power control operations under different conditions providing fast dynamic response and improving the power quality for AC MGs. The overview of proposed control scheme for VSIs of AC MG is illustrated in Fig. 1.

Table 1
Overview of main control schemes for VSIs.

Performance indicators	PI/PID Controllers	Sliding Mode Controllers	Dead-beat Controllers	Artificial Neural Network-based Controllers	Model Predictive Controllers
Theoretical framework	strong	strong	intermediate	low	strong
Computation Burden	limited	intermediate	ordinary	limited	more
Sensitivity metrics	high	robust	ordinary	depends on data	tunable
Tackling Non-linearities	cannot	can	can	can	can
Tackling system constraints	cannot	cannot	cannot	can	can
Intuitive design	limited	intermediate	ordinary	limited	high

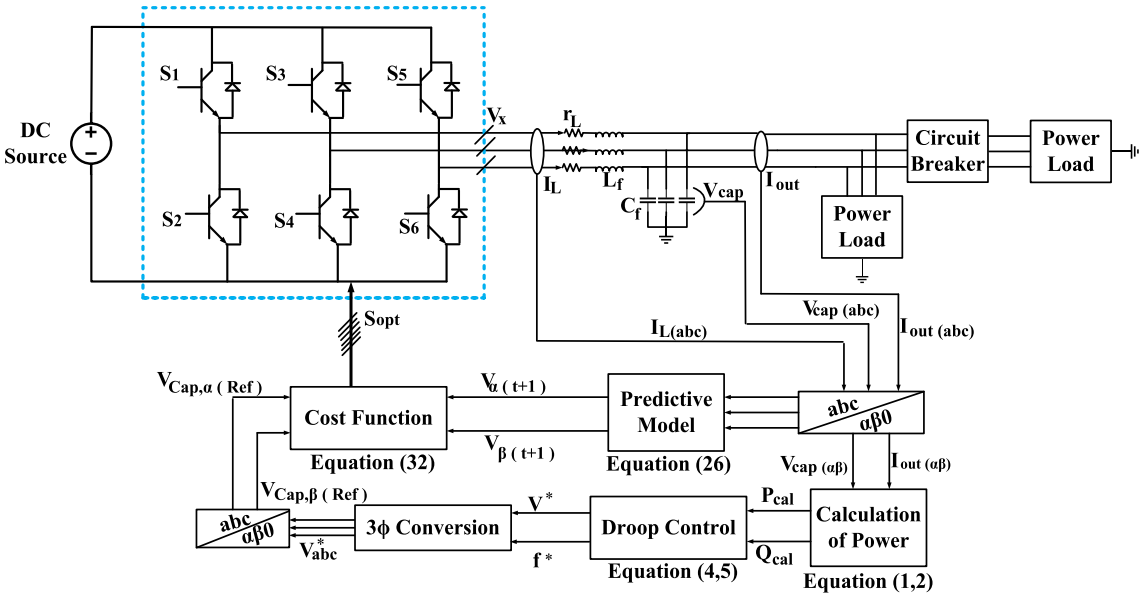

Fig. 1. Circuit diagram of three-phase voltage source converter based on MPC.

2.1. Droop control

Frequency instability is exacerbated by the intermittency and seasonality of the RERs. If VSIs are connected in a parallel way forming a microgrid, then droop control is widely used in power systems to handle the frequency deviation and power sharing between DGs. In the droop control method, first instantaneous active as well as reactive powers are calculated using Equation (1) and (2) from measured output voltage and current.

$$P_{measured} = V_{cap,\alpha} \times I_{out,\alpha} + V_{cap,\beta} \times I_{out,\beta} \tag{1}$$

$$Q_{measured} = V_{cap,\beta} \times I_{out,\alpha} - V_{cap,\alpha} \times I_{out,\beta} \tag{2}$$

A low-pass filter (LPF) is used to reject the main harmonics of measured power. This LPF stops the control mechanism to take action against the transient fluctuations, and the transfer function of the low-pass filter is given in Equation (3). Each DG has its own droop control characteristics to share the power demands accordingly.

$$TransferFunction = \frac{1}{1 + sT_{samp}} \tag{3}$$

The droop control can be represented mathematically by Equations (4) and (5) [61].

$$\omega^{*} = \omega_n - m_p P_c \tag{4}$$

$$V^{*} = V_n - n_q Q_c \tag{5}$$

The angular frequency is regulated from the active power, where reference angular frequency is denoted by ω^*, ω_n represents nominal frequency, frequency droop is denoted by m_p, and change in reactive power and active power is represented by Q_C and P_C respectively. Equation (4) and (5) describe the relation between voltage deviation and output reactive power change. Where actual or controlled voltage is represented by V, the magnitude of nominal (reference) voltage is represented by V*. Then this reference voltage is converted to αβ0 reference frame as depicted in Fig. 2.

3. Mathematical representation of distributed energy resources for VSIs

The schematic of the model predictive controller along with three-phase, two-level VSI under this research study is shown in Fig. 1. Firstly, it is necessary to determine the filter parameters and discrete-time modeling of the power converter because they are required to establish the optimal action as a result of the minimization of CF. This lowest value of CF assists the controller for further control action for the subsequent sampling interval. The optimal performance of the proposed controller is achieved by finding an accurate mathematical representation of the VSI and its filter values. For mathematical modeling of the VSIs, three-phase voltages and currents are converted into two-phase quantities using the αβ0 stationary reference frame, a frequently

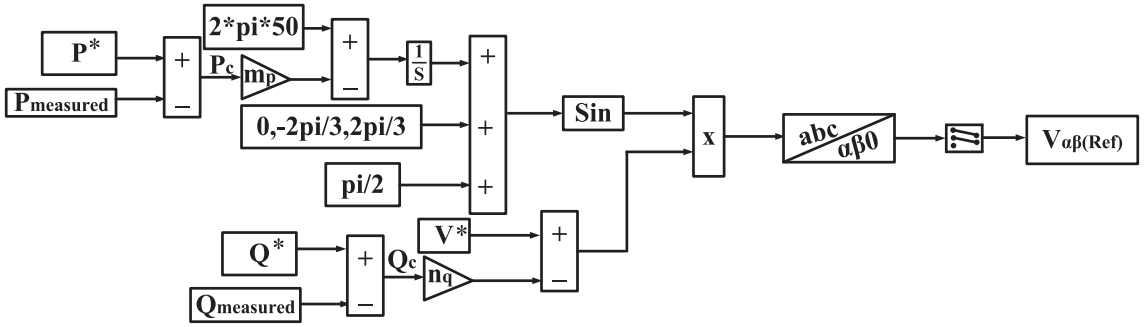

Fig. 2. Droop control and voltage reference generation.

employed method in the control strategies of VSIs.

$$\overline{V} = V_\alpha + jV_\beta = \overline{T}_{samp}[V_a, V_b, V_c] \tag{6}$$

$$\overline{I} = I_\alpha + jI_\beta = \overline{T}_{samp}[I_a, I_b, I_c] \tag{7}$$

where T_{samp} represents the sampling time interval, and it is given by:

$$\overline{T}_{samp} = \frac{1}{3}\left[e^{j2\pi/3} \quad e^{j4\pi/3} \right] \tag{8}$$

This frame of reference is derived from the abc frame of reference using Clarke transformation, and in this frame, the α-axis is obtained from all the three-phase quantities, and the β-axis achieved from two phases, "b" and "c", and then taking a difference from phase "a" and can be written as;

$$V_\alpha = \frac{2}{3}V_a - \frac{1}{3}V_b - \frac{1}{3}V_c \tag{9}$$

$$V_\beta = \frac{2}{3}\left(\frac{-1}{\sqrt{3}}V_b + \frac{1}{\sqrt{3}}V_c\right) \tag{10}$$

The transformation of three-phase quantities to αβ0 frame is necessary to develop smooth and easy control of VSIs. In this way, analysis and control design of the system becomes more straightforward and enables reliable and stable operation in power networks using this transformation as compared to dq0 transformation.

3.1. Modeling of voltage source power converter for AC microgrids

Since there are three legs, S_a, S_b and S_c, for the three-phase VSIs, and each leg is consisted of two switches, and only one switch can be turned on in each leg, so there will be a maximum of two possible switching states for each leg of VSIs as described below in Equation (11)-(13). It is possible to determine the voltage between each leg of VSI and a point N by multiplying the voltages at the DC link (V_{in}) and the present switching state of the corresponding leg of VSIs:

$$S_a = \left\{ \begin{array}{l} 1; SwitchS1isturnedon, whileSwitchS4iskeptoff \\ 0; SwitchS1isturnedoff, whileSwitchS4iskepton \end{array} \right\} \tag{11}$$

$$S_b = \left\{ \begin{array}{l} 1; SwitchS2isturnedon, whileSwitchS5iskeptoff \\ 0; SwitchS2isturnedoff, whileSwitchS5iskepton \end{array} \right\} \tag{12}$$

$$S_c = \left\{ \begin{array}{l} 1; SwitchS3isturnedon, whileSwitchS6iskeptoff \\ 0; SwitchS3isturnedoff, whileSwitchS6iskepton \end{array} \right\} \tag{13}$$

$$V_{aN} = S_a \times V_{in} \tag{14}$$

$$V_{bN} = S_b \times V_{in} \tag{15}$$

$$V_{cN} = S_c \times V_{in} \tag{16}$$

Switching states of all three legs of VSIs, which are found using Clark transformation, are given in Table 2.

Now α-β illustration of the three-phase output voltages for three phases of VSI can be stated in terms of the switching states of three upper-leg switches:

$$\begin{bmatrix} V_\alpha \\ V_\beta \end{bmatrix} = \frac{2}{3}Vin \begin{bmatrix} 1 & -1/2 & -1/2 \\ 0 & \sqrt{3}/2 & -\sqrt{3}/2 \end{bmatrix} \begin{bmatrix} S_a \\ S_b \\ S_c \end{bmatrix} \tag{17}$$

3.2. System dynamics and state space representation

The filter of the VSI is responsible for suppressing switching harmonics and minimizing ripples of current and voltages. This filter is consisted of an inductor (L) and a capacitor (C). The equivalent series resistance of inductor, voltage across capacitor, filter current, and output current are represented by V_{cap}, I_L, and I_{out}. The dynamic behavior of the capacitor and inductor of the LC filter of the VSI as given in Equation (18) and (19):

Table 2
Switching configuration of three phase VSIs.

Vector states	S_a	S_b	S_c	Space Vector	Vectors Placement
	1	0	0	$\overrightarrow{V_1}$	$2V_{in}/3$
	1	1	0	$\overrightarrow{V_2}$	$\frac{V_{in}}{3} + j\frac{V_{in}}{\sqrt{3}}$
Active states	0	1	0	$\overrightarrow{V_3}$	$-\frac{V_{in}}{3} + j\frac{V_{in}}{\sqrt{3}}$
	0	1	1	$\overrightarrow{V_4}$	$-2V_{in}/3$
	0	0	1	$\overrightarrow{V_5}$	$-\frac{V_{in}}{3} - j\frac{V_{in}}{\sqrt{3}}$
	1	0	1	$\overrightarrow{V_6}$	$\frac{V_{in}}{3} - j\frac{V_{in}}{\sqrt{3}}$
Passive states	1	1	1	$\overrightarrow{V_7}$	0
	0	0	0	$\overrightarrow{V_0}$	0

$$C_f\frac{dV_{cap}}{dt} = I_{cap} = I_L - I_{out} \tag{18}$$

$$L_f\frac{dI_L}{dt} = V_x - I_L.r_L - V_{cap} \tag{19}$$

The V_x represents the permissible voltage vectors from the three phase VSI which are provided in Table 2. So, the state-space representation of equations (18) and (19) can be defined as:

$$\frac{dx}{dt} = Ax + By \tag{20}$$

For three-phase VSIs, the values for x, y, A and B are defined as:

$$x = \begin{bmatrix} V_{cap} \\ I_L \end{bmatrix}, y = \begin{bmatrix} V_x \\ I_{out} \end{bmatrix}, A = \begin{bmatrix} 0 & 1/C \\ -1/L & -r_L/L \end{bmatrix}, B = \begin{bmatrix} 0 & -1/C \\ 1/L & 0 \end{bmatrix} \tag{21}$$

3.3. Formulation of cost function

Now, it is necessary to convert the linear differential Equation (18) to a discrete-time domain representation using the forward Euler method because it is compulsory for approximating differential terms with finite differences. Equation (18) can be written in explicit form where the state vector is represented by x(t) and transition matrices are denoted by "A" and "B".

$$x'(t) = A.x(t) + B.y(t) \tag{22}$$

If sampling time (T_{samp}) is taken into consideration with a time step, the discrete time state for the next stage can be written as:

$$x(t+1) = T_{samp}[A.x(t) + B.y(t)] + x(t) \tag{23}$$

Since $e^{T_{samp}\times A} \approx I + T_{samp} \times A$ (24)

Now, after solving Equation (23), it can be written as:

$$\begin{aligned} x(t+1) &= e^{T_{samp}}.x(t) + A^{-1}\left(e^{T_{samp}} - I\right)\begin{bmatrix} B.y(t) \\ 0 \end{bmatrix} \\ &+ A^{-1}\begin{bmatrix} e^{A.T_{samp}} - I & 0 \\ 0 & e^{A.T_{samp}} - I \end{bmatrix}\begin{bmatrix} B.y(t) \\ B.y(t) \end{bmatrix} \end{aligned} \tag{25}$$

Further simplification of Equation (25) yields:

$$x(t+1) = x(t).e^{A.T_{samp}} - B.y(t).A^{-1}\left(I_{2\times 2} - e^{A.T_{samp}}\right) \tag{26}$$

In Equation (26), the identity matrix is denoted by "I" and equation (26) can be described as:

$$x(t+1) = x(t).L - \mathrm{B.y(t)}.M \tag{27}$$

where $L = e^{A.T_{samp}}$ and $M = A^{-1}\left(I_{2\times2} - e^{A.T_{samp}}\right)$ are state transition matrix and impact of regulated input upon individual time step respectively. If $V_{x,\alpha}$ and $V_{x,\beta}$ represent the voltage vectors of different possible switching states of three phase VSI, then in αβ0 frame of reference, it can be written as:

$$V_{x,\alpha} = \frac{2}{3}V_{in}\left[0 \quad 1 \; 1/2 \quad -1/2 \; -1 \quad -1/2 \; 1/2 \quad 0\right] \tag{28}$$

$$V_{x,\beta} = \frac{2}{3}V_{in}\left[0 \quad 0 \; \sqrt{3}/2 \quad \sqrt{3}/2 \; 0 \quad -\sqrt{3}/2 \; -\sqrt{3}/2 \quad 0\right] \tag{29}$$

Now, it is possible to predict the next stage with the help of existing stage as well as possible control action in αβ0 frame of reference using equations (30) and (31).

$$x_{(t+1)\alpha} = e^{T_{samp}.A}\begin{bmatrix} V_{cap,\alpha} \\ I_{L,\alpha} \end{bmatrix} + A^{-1}\left(e^{T_{samp}} - I\right)B\begin{bmatrix} V_{x,\alpha}(t) \\ I_{out,\alpha} \end{bmatrix} \tag{30}$$

$$x_{(t+1)\beta} = e^{T_{samp}.A}\begin{bmatrix} V_{cap,\beta} \\ I_{L,\beta} \end{bmatrix} + A^{-1}\left(e^{T_{samp}} - I\right)B\begin{bmatrix} V_{x,\beta}(t) \\ I_{out,\beta} \end{bmatrix} \tag{31}$$

where "t" represents the chosen switching stage among eight possible switching states of VSI and $V_{cap,\alpha}$ and $V_{cap,\beta}$ represent the existing stage voltages in in αβ0 frame of reference. These predictions are used by MPC algorithms to assess how fine potential control actions are aligning with required reference voltages. After this, it is necessary to formulate the CF to control the capacitor voltage efficiently using reference voltage and voltage of predicted stage.

$$CF = \left(V_{cap,\alpha(Ref)} - V_{cap,\alpha(t+1)}\right)^2 - \left(V_{cap,\beta(Ref)} - V_{cap,\beta(t+1)}\right)^2 \tag{32}$$

3.4. Theoretical analysis of the proposed scheme

After modeling of three phase VSI, its state space representation, developing a discrete time domain model and formulation of cost function, it is necessary to use the discrete time domain model to form a prediction horizon for predicted states. If "A" is discrete time matrix, x(t) is state vector for instant "t", j is time step, the prediction of switching states at the instant "t + j" is represented by $t + j_t$ based on the information existing at instant "t" then predicted horizon will be:

$$x(t + j_t) = A^j x(t) + \sum_{i=0}^{j-1} A^i.B.u(t + j - 1 - i) \tag{33}$$

Now the minimized cost function over the predicted horizon can be written as:

$$J = \sum_{i=0}^{N_P}\left[\left(V_{cap,\alpha(Ref)} - V_{cap,\alpha(t+j_t)}\right)^2 - \left(V_{cap,\beta(Ref)} - V_{cap,\beta(t+j_t)}\right)^2\right] \tag{34}$$

The stability of the system can be assessed using a scalar function called Lyapunov Function which is denoted by V(x). If symmetric definite matrix is denoted by "P" and P > 0 then the performance of a controller is stable if Lyapunov function is decreasing over time and it can be expressed as:

$$V(x(t)) = x\left(t^T\right) \times P.x(t) \tag{35}$$

The Lyapunov function for next sampling instant can be expressed as:

$$V(x(t+1)) = (x(t+1))^T \times P.x(t+1) \tag{36}$$

Using the state equations, the updated equation for Lyapunov function is:

$$V(x(t+1)) = A.x(t) + B.u(t)^T \times P.Ax(t) + B.u(t) \tag{37}$$

Thus, it is concluded that if V(x(t + 1)) – V(x(t)) < 0; then system under MPC is stable. The Lyapunov function helps to analyze the system stability. Assessing the control process effectiveness in MPC for a three-phase VSI involves an investigation that considers several factors such as tracking error, response time and total harmonic distortion (THD). These aspects combined, play a role in determining how the control strategy aligns with the systems operational goals.

4. Performance assessment

4.1. Analysis for VSIs for AC MG

Initially, the individual VSIs for AC MG are simulated in MATLAB / Simulink environment under different load scenarios. The VSIs for proposed AC MG simulated are shown in Fig. 3.

The parameters used for the simulation of individual inverters for AC MG are provided in Table 3.

4.2. Analysis for VSI based on PR controller

Initially the VSIs for proposed AC MG are simulated using PR controller. The VSIs are habitually dependent on RERs. These RERs are non-inertial and usually generate variable power. So, droop control plays a pivotal role for stabilizing frequency to ensure efficient and stable operation. The droop coefficients are denoted by m_p and n_q. The simulation results for individual VSI using PR controller are shown in Fig. 4. It can be observed in Fig. 4 that phase to phase voltages and current are sinusoidal waves initially with some over shoot and under shoot with the resistive load but later on voltages and current are completely sinusoidal.

The output power of resistive load and angular frequency of PR controller based VSI is shown in Fig. 5. The complexity of the control schemes is also reduced using droop control for regulating the frequency in a non-communicative way because it also enables a decentralized control approach where several VSIs can correspondingly share load variations. Moreover, it is specifically advantageous in isolated or remote locations where installing general communication setup is unfeasible.

The voltage stability of the PR controller based VSI is observed by connecting two loads of 7.5 kW, i.e. initially a load of 7.5 kW is connected and after 1.5 s another load of 7.5 kW is connected to observe the behavior of VSI in load transitions as can be seen in Fig. 6. It is evident from Fig. 6 that there is slight fluctuation in voltage for a moment and then PR controller is able to stable the line to line voltages and current is doubled with the addition of second load.

Moreover, when 2nd load is disconnected, the voltage and frequency fluctuations and restorations at 2.5 s can be seen in Fig. 7 and line to line current is restored for RL load of 7.5 kW and 7.5 kVAR. When 2nd load is disconnected, the angular frequency is slightly reduced but droop control performs well and angular frequency remains within tolerable range.

4.3. Analysis for VSI based on MPC

It is evident from Fig. 4 and Fig. 7 that PR controller performs well but it has slightly higher over shoot and undershoot in phase to phase voltages and current and its dynamic response is also slow which can be observed in section 4.2. Therefore, an advanced control scheme based on FCS-MPC is proposed for VSIs of AC MG to reduce overshoot and undershoot in phase to phase voltages to get stable and smooth voltages with quick dynamic response for load transitions. It can be observed in Fig. 8 that when a resistive load is connected, the MPC based VSI provides the output phase to phase voltages with negligible overshoot or undershoot 5 milli seconds.

The output power and behavior of frequency for single purely resistive load of simulated MPC based VSI is shown in Fig. 9.

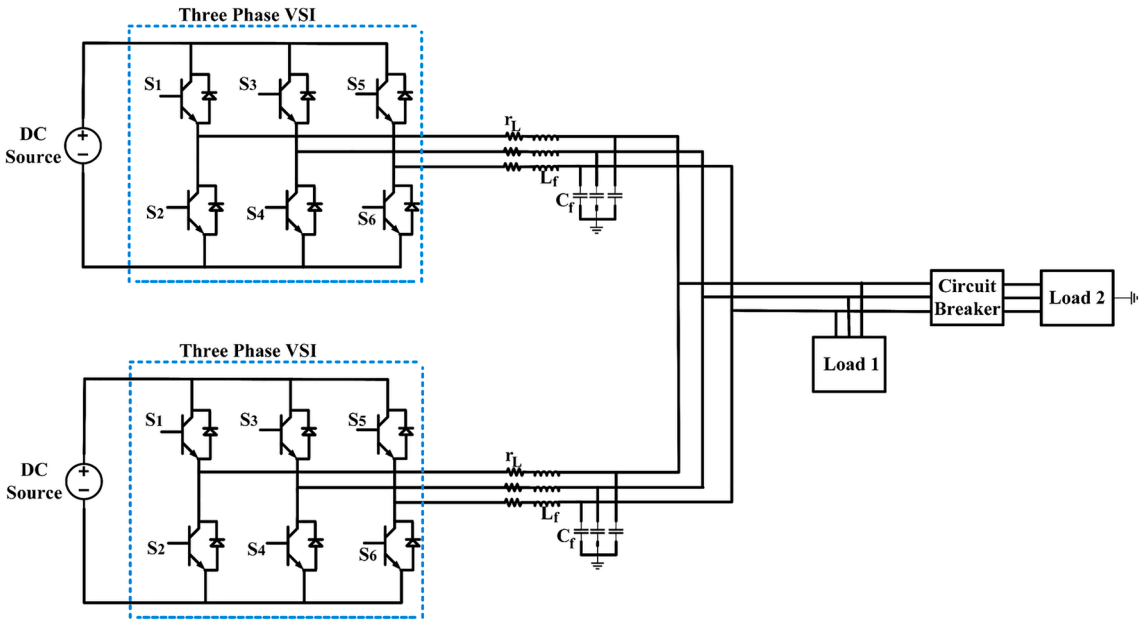

Fig. 3. VSIs dominated AC MG.

Table 3
Simulation parameters for VSIs in AC MG.

Parameters	Values
Input voltage	1000 V
Sampling time	1 μS
Capacitor	16 μF
Inductor	13 mH
Equivalent series resistance of inductance	0.7 mΩ
AC disturbance voltage in input dc voltage	80 V
Resistive load 1	15 kW
Resistive load 2	15 kW
RL load 1	15 kVAR
RL load 2	15 kVAR
Nonlinear load 1 (bridge rectifier with resistive load)	9 Ω
Nonlinear load 2 (bridge rectifier with resistive load)	5 Ω
System frequency	50 Hz
Droop coefficients	$m_p = 0.000014$, $n_q = 0.000014$
Phase to phase output voltage	326 V

4.4. Characterization of load transitions for individual inverter

In order to confirm the robustness of proposed control scheme, each inverter should be tested with single load and multiple loads up to 15 kW. Therefore, each VSI is connected to a 7.5 kW initially and later on, another load of 7.5 kW is also connected, and output phase to phase voltage and current across the loads are observed to see the behavior of the controller during load transitions. Fig. 10 depicts that the proposed controller shows a quick dynamic response during load transition with smooth output voltage and load current. When a load 7.5 kW is connected, inverter is providing 46 A current and an output phase to phase voltage of 326 V across the load, but with the addition of 2nd load of 7.5 kW, the inverter is smoothly providing 92 A current and 326 V across load. Fig. 10 depicts that the proposed controller shows an immediate response during load transition with smooth current and voltages to the terminal load. From the above discussion, it is clear that individual VSIs are capable of handling the load demand of 15 kW with the proposed control scheme. Then, several tests, like variation of loads and addition of AC voltage as a disturbance in the DC input voltage are performed to confirm the robustness and stability of the proposed control scheme during steady state operation.

After this, the behavior of proposed control scheme is validated for resistive-inductive (RL) loads because RL load characterized by its resistive and inductive properties, exhibits explicit challenges for instance, slower response time due to inductance and potential for oscillations where RL load demanding 7.5 kW active power and 7.5 kVAR reactive power is connected to VSI as depicted in Fig. 11. The MPC considers these characteristics inherently in its predictive model.

The key advantage of MPC is its ability to handle multiple control objectives simultaneously, such as sustaining the output voltage at the anticipated level, minimizing the current ripple, and confirming effective operation of the VSIs.

4.5. Comparison of performance for PI, PR and MPC based VSI

If a battery of 1.2 Ah is connected as a voltage source with VSI, the VSI is tested for PI and PR based control scheme to analyze its performance and depth of discharge (DOD) based on PI and PR controller at 40 % state of charge (SOC) of battery. It is evident from Fig. 12 and Fig. 13 that if a resistive load of 10 kW power is connected then using PI and PR controller, VSI looses its power rating at approximately 30 s where DOD of battery is approximately 70 % and 69 % respectively.

The parameters of battery used in simulation to see performance of PR controller are given in Table 4.

Now the simulation results for MPC based VSI are shown in Fig. 14 to observe the DOD of battery and VSIs continue to work with the rated power up to 72 % of DOD of battery.

The performance of MPC based VSI in order to overcome the overshoot, undershoot, dynamic response, load transitions and % THD is better than PR controller based VSI., therefore MPC based control scheme was utilized and further studied for standalone AC MG.

4.6. Analysis of standalone AC MG under steady-state conditions

Eventually two DGs having VSIs are connected in a parallel way, forming a stand-alone MG as shown in Fig. 3, then droop control has been used as a primary controller, while MPC is implemented to regulate the output voltage of the AC MG. In the MGs, the control strategy of the GFM converters is based on a closed-loop control to keep the load voltages stable. Simulation results for phase to phase voltages across

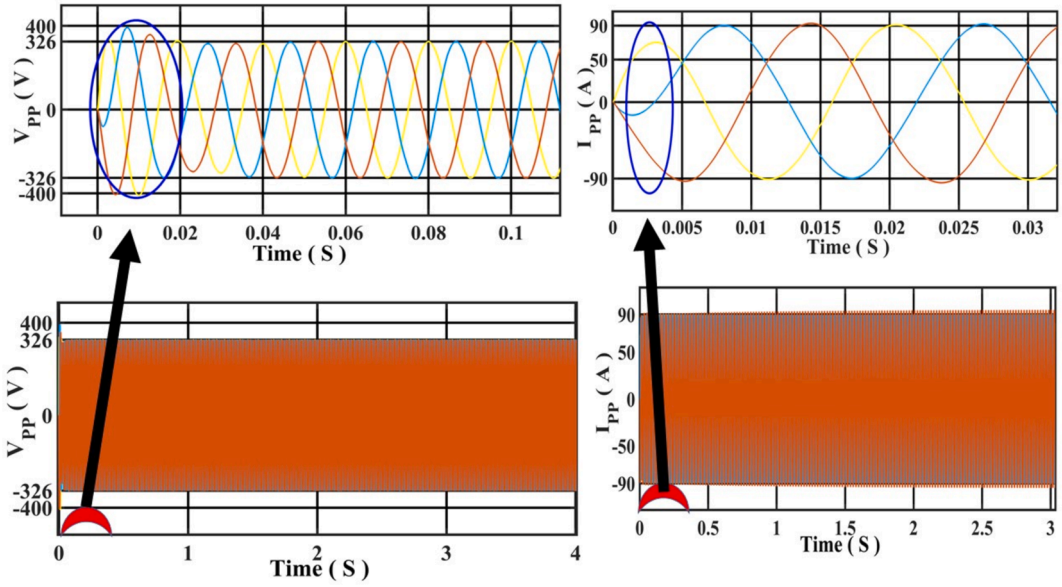

Fig. 4. Line to line voltage and current for 15 kW load from individual VSI in AC MG.

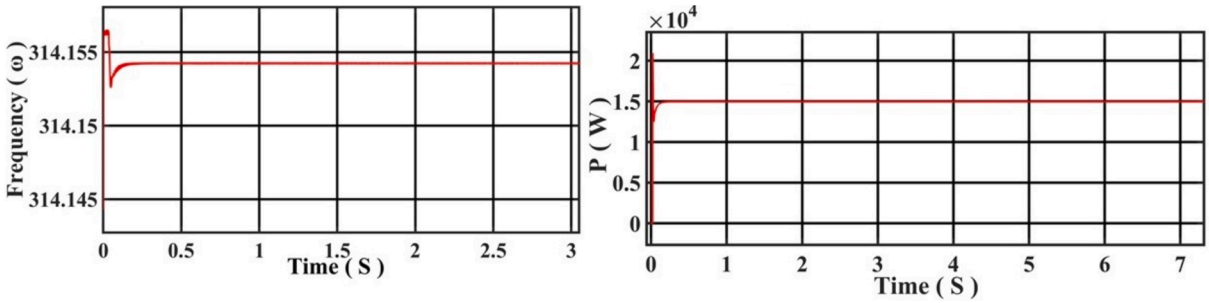

Fig. 5. Angular frequency and output power of resistive load for individual VSI.

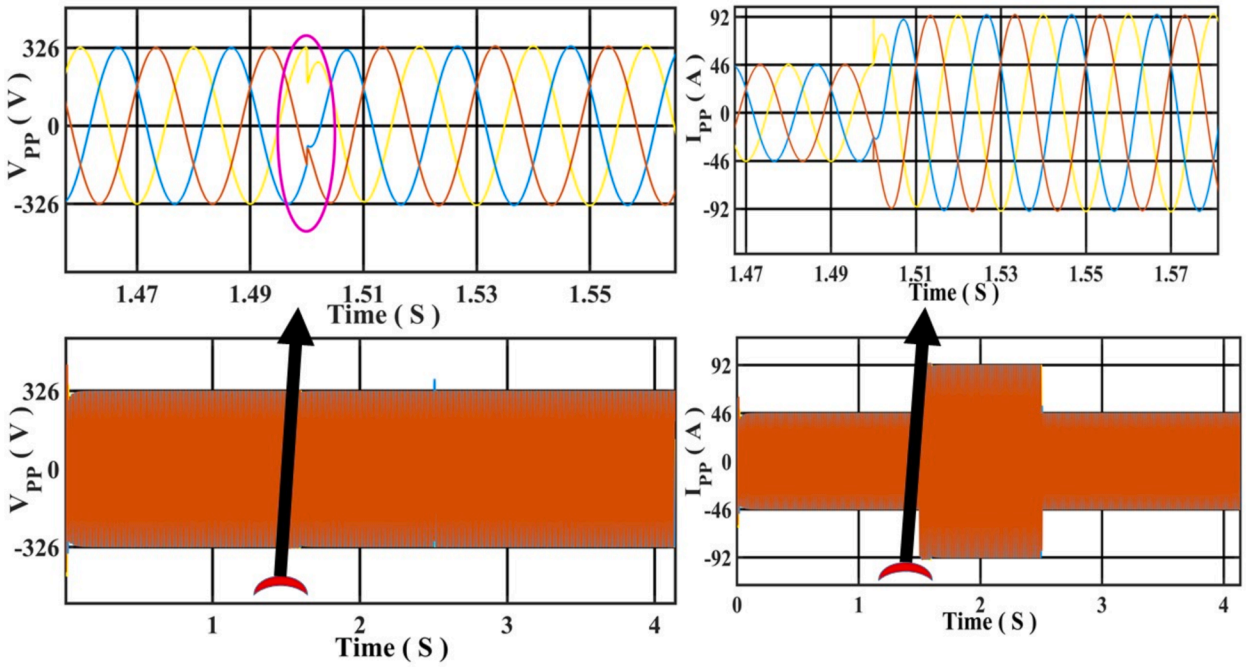

Fig. 6. Line to line voltage and current for load transitions at individual VSI.

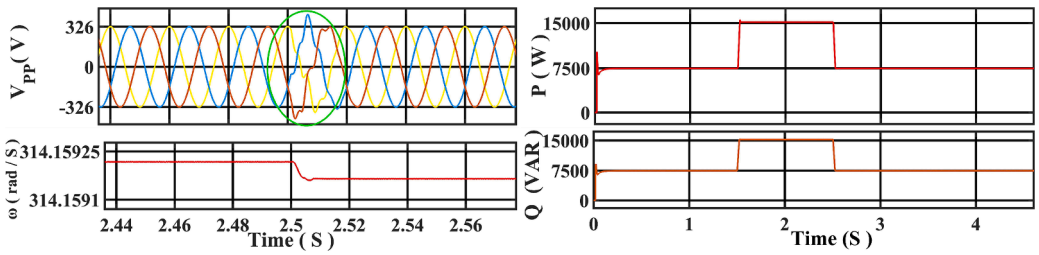

Fig. 7. Line to line voltage and frequency behavior during high load to low load transitions.

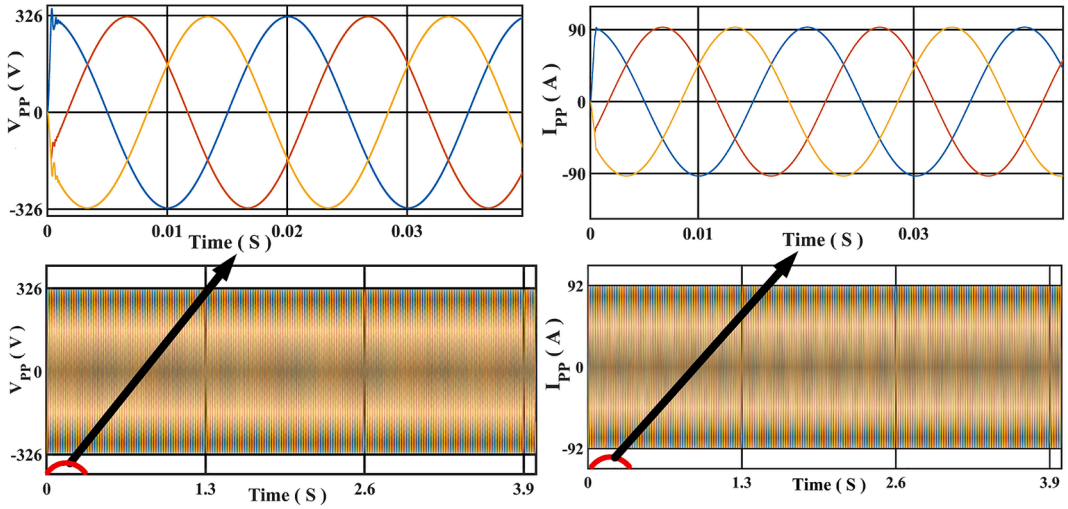

Fig. 8. Phase to phase voltage and current for 15 kW load from individual VSI in AC MG.

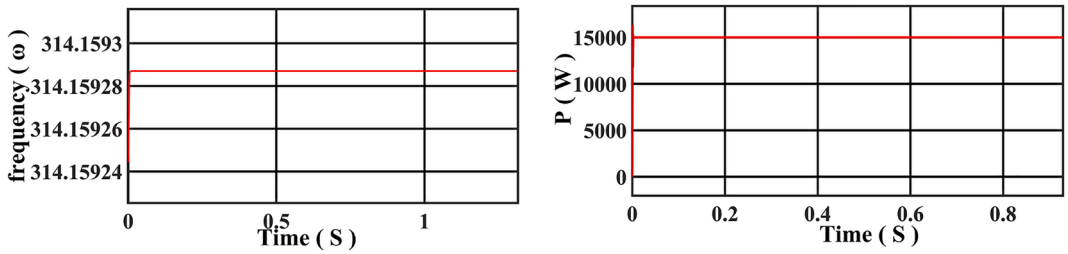

Fig. 9. Simulation results for Frequency and Power with 15 kW load.

load in the stand-alone operation of AC MGs are presented in Fig. 15 under normal operational situations and load transitions when two loads are connected in the AC MG.

The two VSIs are connected in a parallel fashion, so their currents are added up at point of common coupling (PCC) and then provided to the load as shown in Fig. 15. Moreover, it is also depicted in Fig. 15 the required load current of 92 A and phase to phase voltage of 326 V are stable and smooth. Similarly, If RL load demanding 15kw active power and 15 kVAR reactive power is connected at the PCC, then the frequency, output voltage, active power and reactive power for RL load of AC MG are shown in Fig. 16.

Fig. 16 shows that the phase to phase voltage at the load side is stable with a load of 15 kw power rating.

4.7. Characterization of load transitions for AC MG

The load transient analysis is performed for parallel connected inverters in this section. Initially, a single load of 15 KW is connected to AC MG. Then, at T = 1.5 s, an additional load is connected, and it can be seen that the output current and voltages are stable, and there is a smooth transition with increased load. The steady and stable output voltage and load current can be observed in Fig. 17.

Finally, the second load is again disconnected at T = 2.5 s, and simulation results can be observed in Fig. 18 for parallel connected VSIs in the stand-alone operation of AC MG.

The AC MG is also tested for RL loads, the active power, reactive power and frequency for RL load can be seen in Fig. 19.

In addition to this, verifying the performance of the standalone AC MGs control strategy with nonlinear loads is vital due to the inimitable challenges and influences that nonlinear loads instigate in the power systems. Therefore, nonlinear loads and their transitions are also established for AC MG. The existence of nonlinear loads for VSIs eminently influences the validation of control schemes of VSI because nonlinear loads generally produce harmonics because of their distorted or non-sinusoidal current draw. Therefore, MPC based VSIs are also tested for nonlinear loads as shown in Fig. 20.

It can be observed in Fig. 20 that a nonlinear load is significantly creating distortion in the current. This non-sinusoidal current drawn can

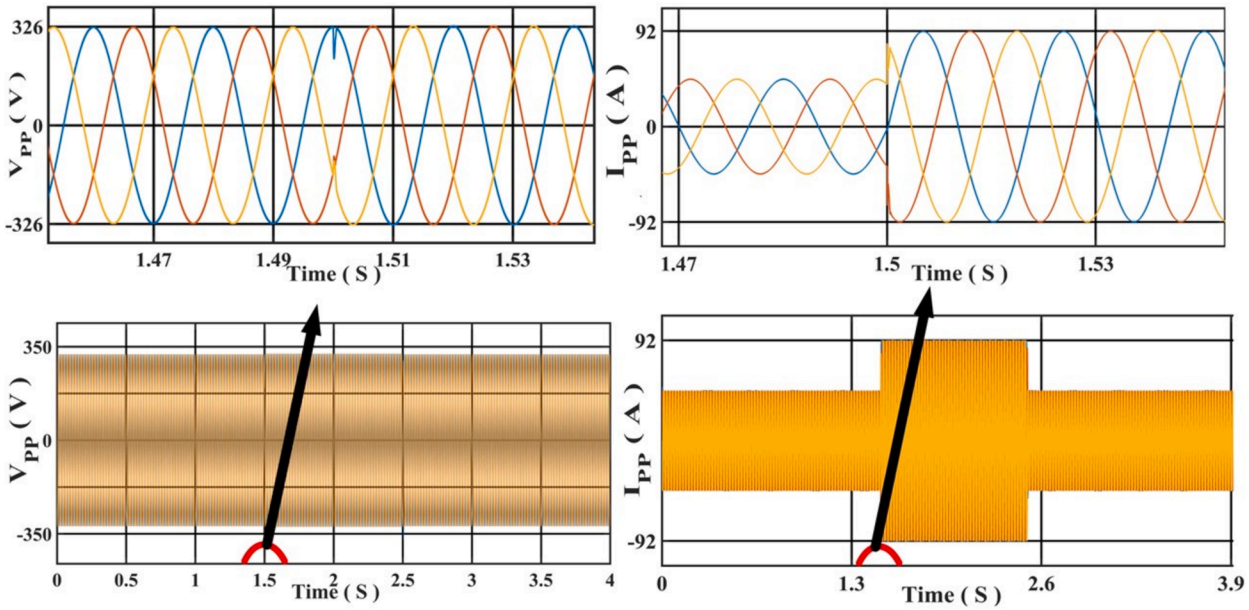

Fig. 10. Phase to phase output voltage and current for load transitions at individual VSI.

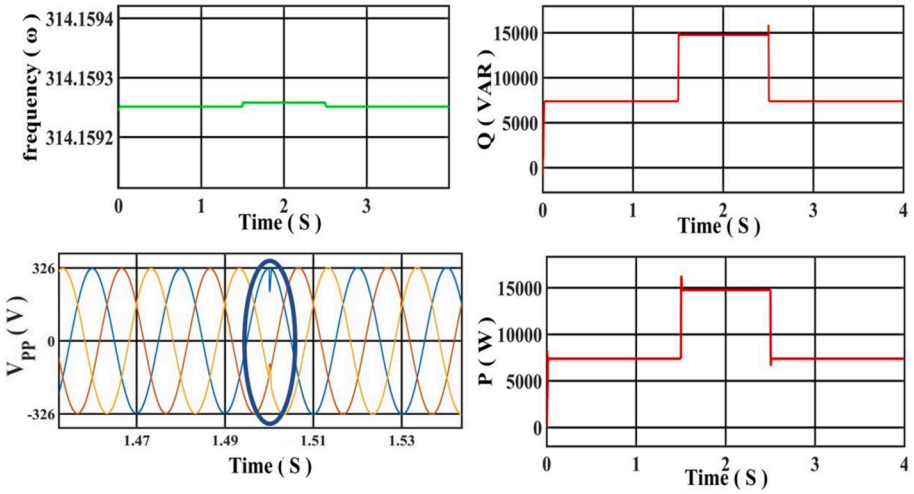

Fig. 11. Behavior of output phase to phase voltage, active power, reactive power and frequency for load transitions at individual VSIs.

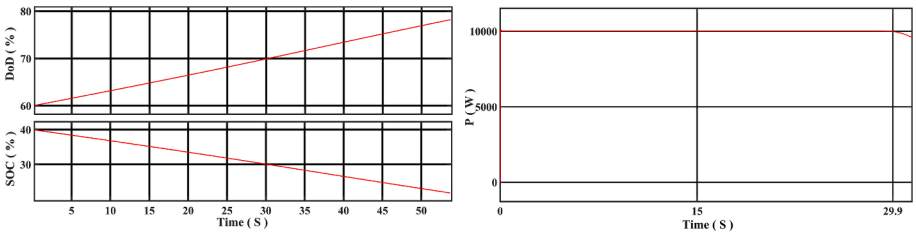

Fig. 12. Behavior of VSI with discharging a battery at initial SOC of 40 % using PI controller.

significantly introduce instabilities in the output voltages of the AC MGs if the control scheme is not advanced and well designed, but it can be seen in Fig. 21 that MPC based control scheme provides an efficient method for managing the overall system's dynamics and voltage stability. Initially, the connected nonlinear load is drawing and 46 A till 1.5 s and then another nonlinear load is added and now there is 92 A current due to two nonlinear loads. Finally, at 2.5 s the second nonlinear load is disconnected as it can be seen in Fig. 20. The simulation results for the behavior of frequency of the overall line to line current in AC MG system can also be observed in Fig. 20 during nonlinear load transitions.

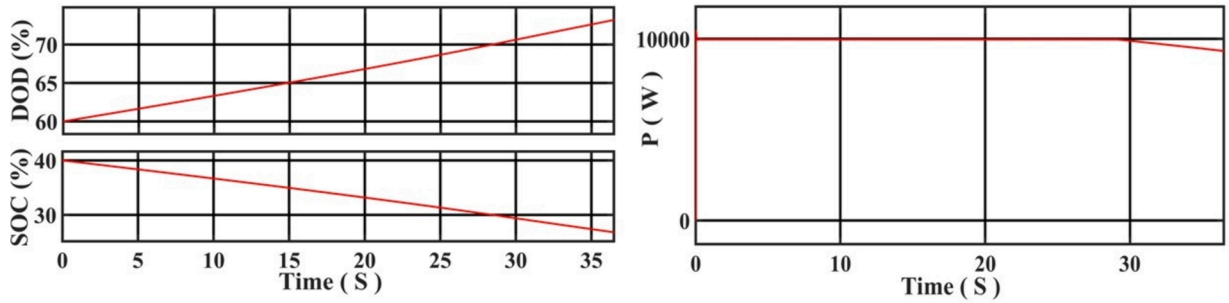

Fig. 13. Behavior of VSI with discharging a battery at initial SOC of 40 % using PI controller.

Table 4
Parameters of battery.

Parameter	Notation	Value	Unit
Initial State of charge	SOC	40	%
Battery response time	–	0.001	S
Rated capacity	–	1.2	Ah
Nominal voltage	V_{dc}	1000	V

Nonlinear loads can cause significant frequency and voltage fluctuations, which the MPC counters by adjusting the operation of inverters as can be noticed in Fig. 20 and Fig. 21. By opting its predictive capabilities and dealing multiple control objectives, the MPC can effectively manage the complexities introduced by nonlinear loads, ensuring reliable and stable voltages in the microgrid. Thus, MPC-based control system for a VSIs in an AC MG with nonlinear loads can effectively provide stable output voltages. Its predictive capabilities, ability to handle rapid load fluctuations, multi-objective optimization, and respect for operational constraints make this control scheme a robust and reliable control strategy for managing the challenges posed by nonlinear loads in microgrids which results in regulating line to line output voltage, and mitigating harmonic distortions caused by the nonlinear loads as shown in Fig. 21. The THD investigations, particularly regarding output voltages in the standalone AC MGs, when having multiple linear and nonlinear loads is necessary to confirm the power quality assessment. The output current is in proportion to the voltage in case of linear loads, ensuing in a sinusoidal current waveform which is inherently in phase with the voltage for GFM VSIs in the AC MGs. In this situation, the primary concern for THD is naturally external, stemming from the supply side. Thus, with linear loads, an MPC-based control

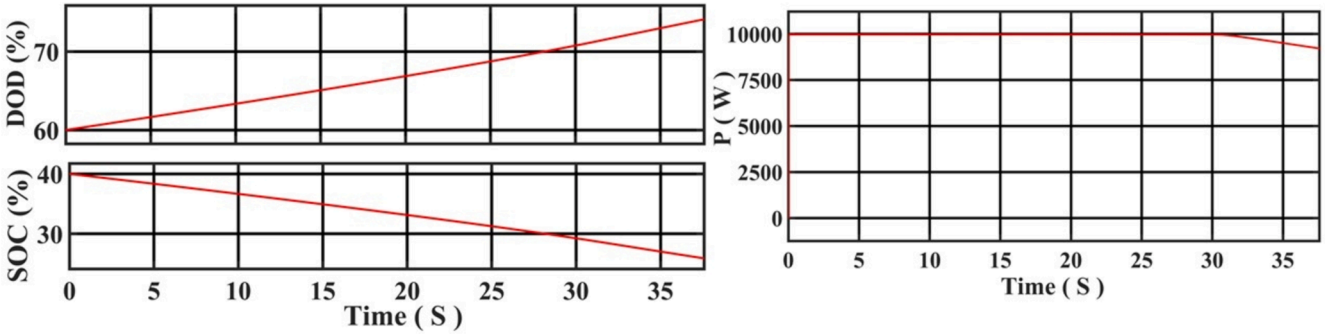

Fig. 14. Behavior of VSI with discharging a battery at initial SOC of 40 % using MPC.

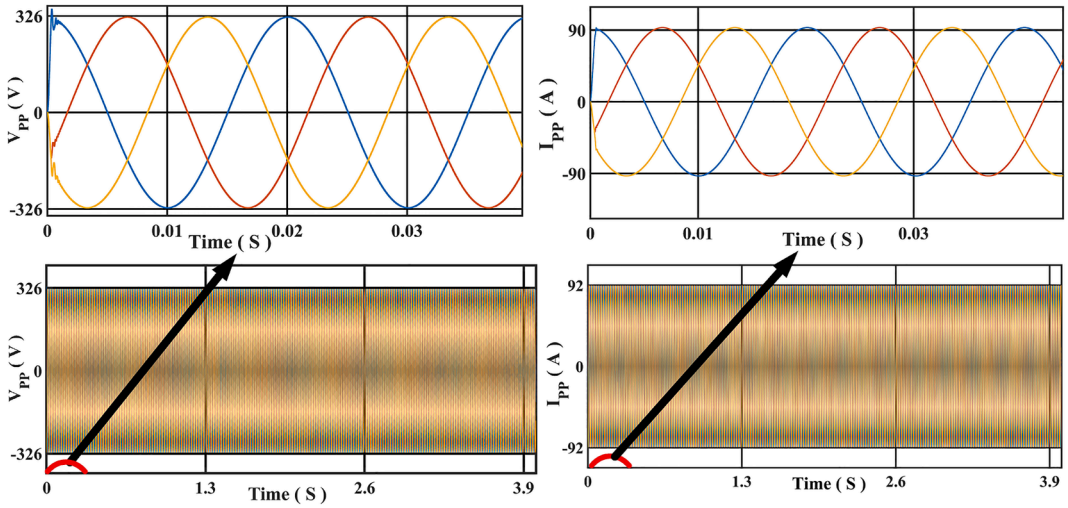

Fig. 15. Phase to phase voltage and current of Grid-forming VSIs with single load.

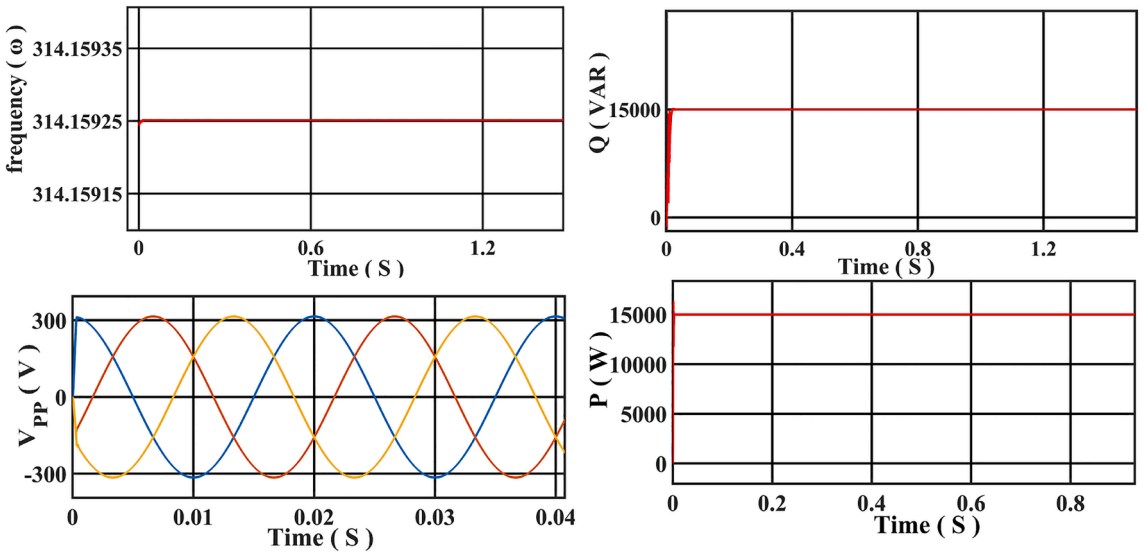

Fig. 16. Output phase to phase voltage, reactive power, active power and frequency of Grid-forming VSIs of AC MG with single load.

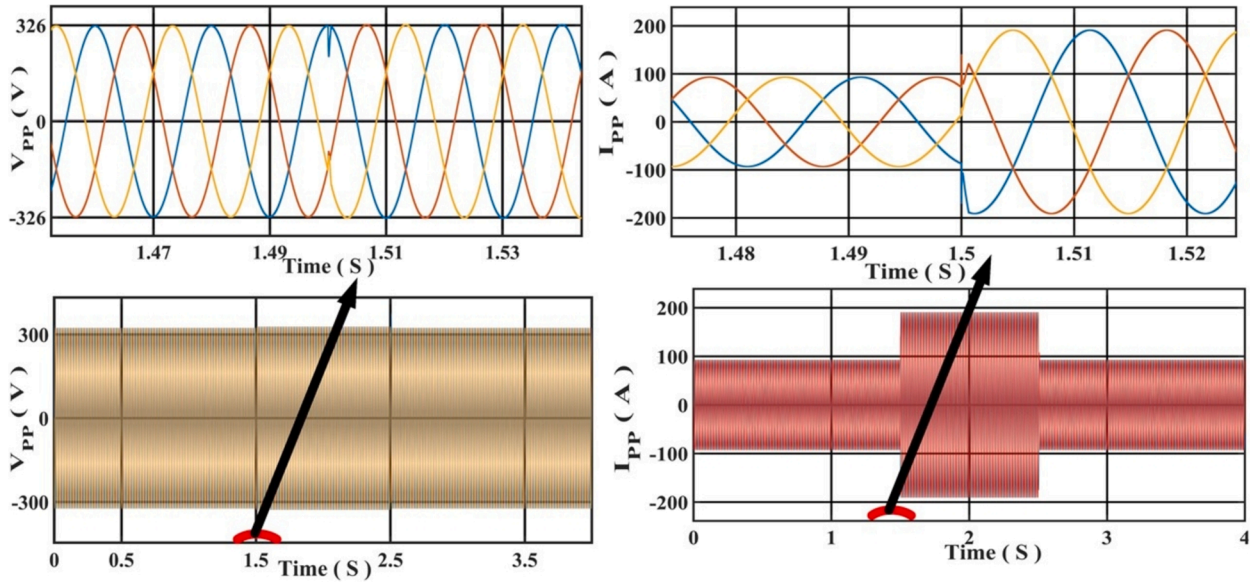

Fig. 17. Output voltage and current with two loads.

scheme primarily focuses on recompensing for any harmonic distortion initiating from the power generation sources. Keeping this point in mind, the AC MG was also tested by adding a disturbance of 80 V AC voltages in the supply side to observe the behavior of the proposed MPC for the standalone AC MG.

It was observed that the MPC can predict and adjust the operations of inverter-based power generation sources within the MG to diminish the impact of these harmonics, guaranteeing that the voltage supplied to linear loads remains entirely sinusoidal as well as stable. On the other hand, nonlinear loads intrinsically draw current in a non-sinusoidal way. This non-linear current draw introduces harmonics into the power system, impacting the THD levels. In these cases, the role of MPC becomes more complex as well as critical. It must uninterruptedly forecast the current harmonics generated by nonlinear loads and dynamically control the VSIs to respond these harmonics to deliver stable and smooth output voltages. In the proposed control scheme the THD of the output voltage for linear and nonlinear loads in these simulation results is 0.86 % and 0.98 % respectively, that is quite fine and in accordance with IEEE standards and codes. The THD for linear and nonlinear loads using improved FCS-MPC for AC MG can be observed in Fig. 22.

The performance analysis of different control schemes based on their THD and the complexity of implemented controllers is summarized in Table 5. Table 5 illustrates that the proposed control strategy exhibits lower THD as compared to other methods proposed in the literature.

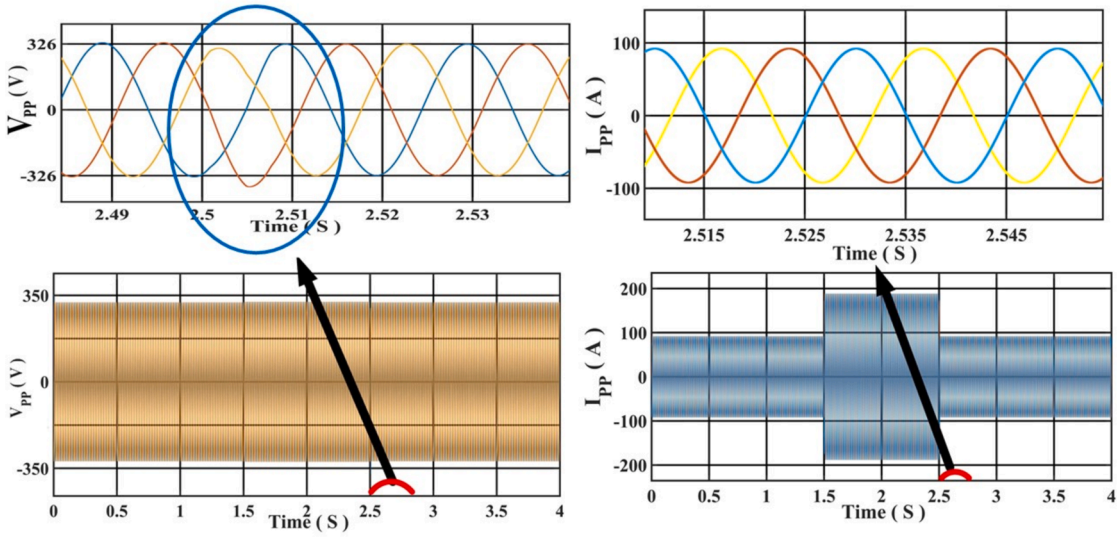

Fig. 18. Line to line voltage and current during load transitions.

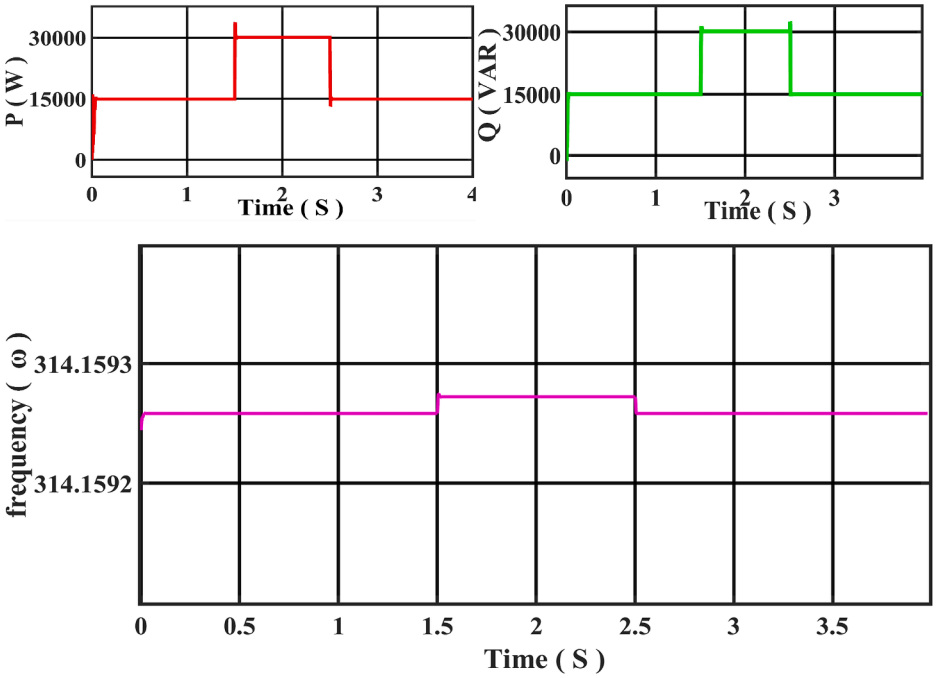

Fig. 19. Simulation results for active power, reactive power and frequency during load transitions using RL loads.

4.8. Transient performance and key performance indicators

Since the purpose is to achieve rapid and robust transient responses during transient operations. The proposed control scheme has been effective in maintaining accurate tracking performance even in the event of challenging transient periods during load transitions. The robustness of the proposed control scheme can be depicted by the fact that it allows for tracking performance to remain during transients which implies that minimal changes in dynamic conditions are experienced by the system thus preserving the performance index with quick dynamic response. This feature is essential for reliability as well as better efficiency of the MGs system at different operating conditions. The key performance indicators of the proposed control scheme are summarized in Table 6.

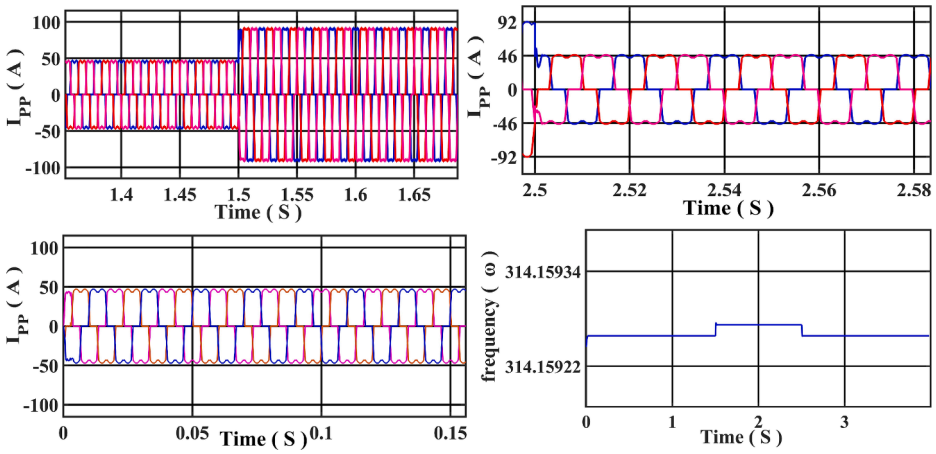

Fig. 20. Behavior of output current and frequency with nonlinear load transitions in AC MG.

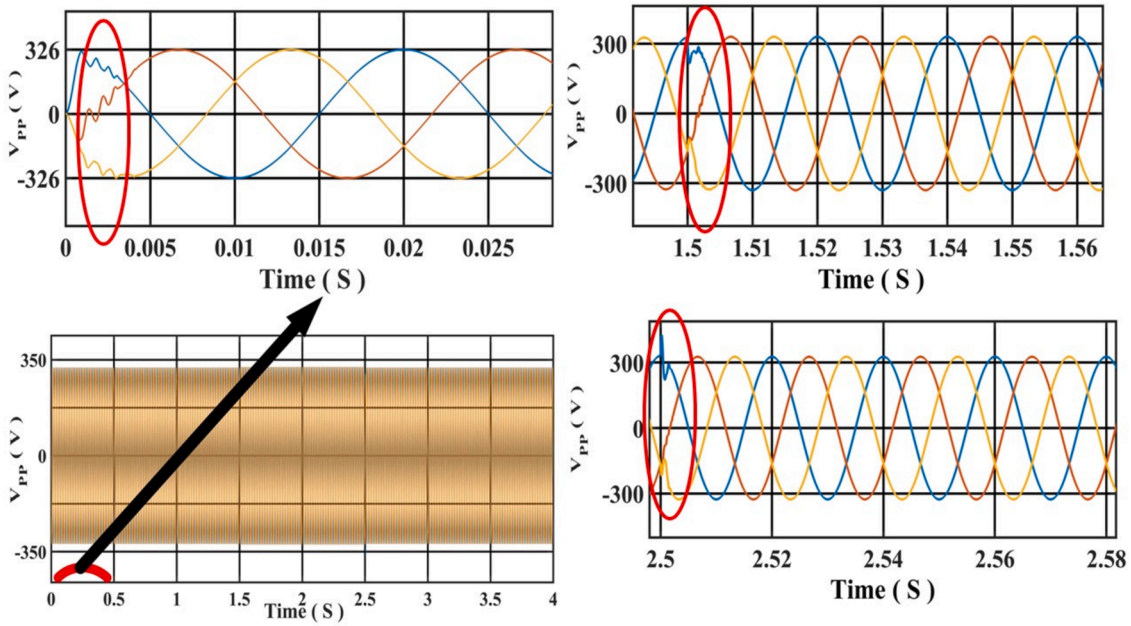

Fig. 21. Simulation results for enhanced voltage stability with nonlinear loads.

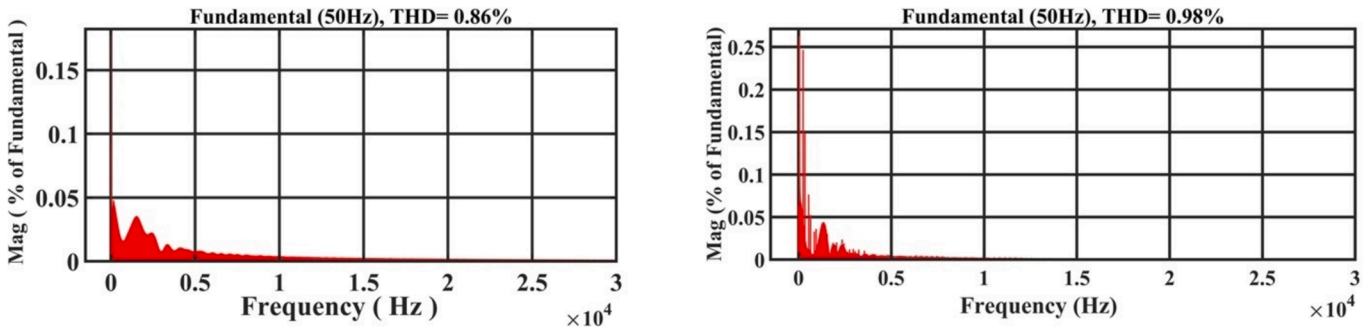

Fig. 22. THD analysis for linear and nonlinear loads.

Table 5
Comparative analysis of distinct control schemes.

References	Control scheme	% THD of VoltagesLinear Load	Nonlinear Load	Complexity of Implemented Controller	Applications
[62]	PI	2.92	Not studied	elementary	DG applications
[63]	PR	1.5	4.9	elementary	UPS, MGs
[64]	SMC	Not studied	2.66	more	UPS, MGs
[65]	Hysteresis MPC	4.19	Not studied	moderate	General MGs
[66]	Observer-based MPC	2.82	3.8	moderate	UPS, MGs
[67]	Improved FCS-MPC	1.06	Not studied	moderate	VSIs for General MGs
[68]	MPC	0.98	Not studied	moderate	VSIs for islanded MGs
[69]	Impedance based control	Not studied	2.27	moderate	VSIs for islanded MGs
[70]	MPC	1.22	Not studied	more	VSIs for DGs
[Proposed]	FCS-MPC	0.86	0.98	moderate	VSIs for standalone MGs

Table 6
Key performance indicators (KPIs).

KPI name	Value	Unit
Initial response time	< 5	milli seconds
Response time from low R load to high R load	2	milli seconds
Response time from low R load to RL load	Immediately	–
Response time from low RL load to R load	10	milli seconds

5. Conclusion

The control scheme based on PR controller, PI controller and FCS-MPC, along with droop control for individual VSIs was thoroughly investigated and based on the performance of MPC for VSI, the operation of standalone AC MGs for different varying loads was completely studied. The performance verification of controller was studied with extensive testing in the MATLAB/Simulink environment. The proposed control scheme was successfully pre-calibrated for a wide range of conditions, including enhanced voltage regulation, precise power sharing, and fast dynamic response for rapid load variation or transient conditions. The prediction for the variables to be controlled is realized by modeling the overall system. The proposed controller is supported on a discrete set of voltage vector, it provides gate signals for switching of the VSIs of AC MG and there is no need of any extra modulator. These voltage vectors describe a particular aggregation of switching states of VSIs. There is no need of traditional cascaded outer-inner loop configuration because the output voltage is directly regulated in this control scheme, resulting in a great simplification of controller design and easier retrofit to industrial controllers. The proposed approach also satisfies the international grid codes and standards in terms of voltage stability and total harmonic distortion of output voltages in steady state and transient load states. In future work, an advanced control approach for three phase VSIs can be designed and developed that will enable the same VSIs of AC MG to work in islanded mode and grid following mode and the controller hardware in the loop testing can also be realized.

CRediT authorship contribution statement

Qudrat Ullah: Writing – review & editing, Writing – original draft, Visualization, Validation, Software, Methodology, Conceptualization. **Enio Costa Resende:** Writing – review & editing. **Luiz Carlos Gomes Freitas:** Writing – review & editing. **Hannu Laaksonen:** Writing – review & editing, Supervision. **Marcelo Godoy Simões:** Writing – review & editing, Supervision, Conceptualization, Methodology, Formal analysis, Proofreading, and Modification for the final layout.

Declaration of competing interest

The authors declare that they have no known competing financial interests or personal relationships that could have appeared to influence the work reported in this paper.

Data availability

No data was used for the research described in the article.

References

[1] Mumtaz F, et al. A Kalman filter-based protection strategy for microgrids. IEEE Access 2022;10:73243–56. https://doi.org/10.1109/ACCESS.2022.3190078.
[2] Li Y, Xia Y, Ni Y, Peng Y, Feng Q. Transient stability analysis for grid-forming VSCs based on nonlinear decoupling method. Sustain 2023;15(15). https://doi.org/10.3390/su151511981.
[3] Green M. Community power. Nat Energy 2016;1(3):1–4. https://doi.org/10.1038/nenergy.2016.14.
[4] Ullah Q, Busarello TDC, Brandao DI, Simões MG. Design and performance evaluation of SMC-based DC–DC converters for microgrid applications. Energies 2023;16(10). https://doi.org/10.3390/en16104212.
[5] D'Adamo I, Mammetti M, Ottaviani D, Ozturk I. Photovoltaic systems and sustainable communities: new social models for ecological transition. The impact of incentive policies in profitability analyses. Renew Energy 2023;202:1291–304. https://doi.org/10.1016/j.renene.2022.11.127.
[6] Olabi AG, et al. Wind energy contribution to the sustainable development goals: case study on London array. Sustain 2023;15(5). https://doi.org/10.3390/su15054641.
[7] Zhang Z, et al. Advances and opportunities in the model predictive control of microgrids: Part I–primary layer. Int J Electr Power Energy Syst 2022;134:107411. https://doi.org/10.1016/j.ijepes.2021.107411.
[8] Mumtaz F, Imran K, Rehman H, Bukhari SBA. 1D recursive median filter based passive islanding detection strategy for grid-connected distributed generations network. IET Renew Power Gener 2023;17(7):1731–46. https://doi.org/10.1049/rpg2.12708.
[9] Souza MET, Freitas LCG. Grid-connected and seamless transition modes for microgrids: an overview of control methods, operation elements, and general requirements. IEEE Access 2022;10:97802–34. https://doi.org/10.1109/ACCESS.2022.3206362.
[10] Li Q, Peng C, Wang M, Chen M, Guerrero JM, Abbott D. Distributed secondary control and management of islanded microgrids via dynamic weights. IEEE Transactions on Smart Grid 2018;10(2):2196–207. https://doi.org/10.1109/TSG.2018.2791398.
[11] Mohamed Y, E. E.-S.-I. T. on Power, and undefined 2008. Adaptive decentralized droop controller to preserve power sharing stability of paralleled inverters in distributed generation microgrids. *ieeexplore.ieee.org*, Accessed: Feb. 03, 2023. [Online]. Available: https://ieeexplore.ieee.org/abstract/document/4696040/.
[12] Wu T, Bao G, Chen Y, … J. S.-C. C. C., and undefined 2018. A review for control strategies in microgrid. ieeexplore.ieee.org, Accessed: Feb. 03, 2023. [Online]. Available: https://ieeexplore.ieee.org/abstract/document/8482549/.
[13] Yazdanian M, Mehrizi-Sani A. Distributed control techniques in microgrids. IEEE Trans Smart Grid Nov. 2014;5(6):2901–9. https://doi.org/10.1109/TSG.2014.2337838.
[14] Mokhtari K, Shokri-Kojori S, Aliyari-Shoorehdeli M. A new generalized state-space averaged model, control design and stability analysis for three phase grid-connected quasi-Z-Source inverters. Int J Electr Power Energy Syst 2024;158:109932. https://doi.org/10.1016/j.ijepes.2024.109932.
[15] Zainab F, et al. An optimal joint planning of DGs and electric vehicle charging stations in grid-connected and islanded microgrids. IET Renew Power Gener 2023;17(7):1623–34. https://doi.org/10.1049/rpg2.12686.
[16] Mumtaz F, Imran K, Abusorrah A, Bukhari SBA. An extensive overview of islanding detection strategies of active distributed generations in sustainable microgrids. Sustain 2023;15(5). https://doi.org/10.3390/su15054456.

[17] Gurugubelli V, Ghosh A. Control of inverters in standalone and grid-connected microgrid using different control strategies. World J Eng 2022;19(5):675–88. https://doi.org/10.1108/WJE-09-2020-0432.
[18] Vikash G, Ghosh A, Rudra S. Integration of distributed generation to microgrid with virtual inertia. In: 2020 IEEE 17th India council international conference (INDICON). IEEE; 2020. p. 1–6. https://doi.org/10.1109/INDICON49873.2020.9342377.
[19] Opiyo NN. A comparison of DC- versus AC-based minigrids for cost-effective electrification of rural developing communities. Energy Rep Nov. 2019;5:398–408. https://doi.org/10.1016/J.EGYR.2019.04.001.
[20] Dragicevic T. Model predictive control of power converters for robust and fast operation of AC microgrids. IEEE Trans Power Electron 2018;33(7):6304–17. https://doi.org/10.1109/TPEL.2017.2744986.
[21] EL-Kholy EE, EL-Sabbe A, El-Hefnawy A, Mharous HM. Three-phase active power filter based on current controlled voltage source inverter. Int J Electr Power Energy Syst 2006;28(8):537–47. https://doi.org/10.1016/j.ijepes.2006.01.007.
[22] Silva M, Morais H, Vale Z. An integrated approach for distributed energy resource short-term scheduling in smart grids considering realistic power system simulation. Energy Convers Manage 2012;64:273–88. https://doi.org/10.1016/j.enconman.2012.04.021.
[23] Lasseter RH. Smart distribution: coupled microgrids. Proc IEEE 2011;99(6):1074–82. https://doi.org/10.1109/JPROC.2011.2114630.
[24] Gurugubelli V, Ghosh A, Panda AK. Parallel inverter control using different conventional control methods and an improved virtual oscillator control method in a standalone microgrid. Prot Control Mod Power Syst 2022;7(1). https://doi.org/10.1186/s41601-022-00248-9.
[25] Gurugubelli V, Ghosh A, Panda AK. A new virtual oscillator control for synchronization of single-phase parallel inverters in islanded microgrid. Energy Sources Part A Recover Util Environ Eff 2022;44(4):8842–59. https://doi.org/10.1080/15567036.2022.2126560.
[26] Gurugubelli V, Ghosh A, Panda AK, Rudra S. Implementation and comparison of droop control, virtual synchronous machine, and virtual oscillator control for parallel inverters in standalone microgrid. Int Trans Electr Energy Syst 2021;31(5):1–26. https://doi.org/10.1002/2050-7038.12859.
[27] Engler A, Soultanis N. Droop control in LV-grids. In: 2005 International Conference on Future Power Systems. IEEE; 2005. 6-pp. https://doi.org/10.1109/FPS.2005.204224.
[28] Shan Y, Hu J, Li Z, Guerrero JM. A model predictive control for renewable energy based AC microgrids without any PID regulators. IEEE Trans Power Electron 2018;33(11):9122–6. https://doi.org/10.1109/TPEL.2018.2822314.
[29] Nguyen TT, Yoo HJ, Kim HM. Application of model predictive control to bess for microgrid control. Energies 2015;8(8):8798–813. https://doi.org/10.3390/en8088798.
[30] Taher AM, Hasanien HM, Ginidi AR, Taha ATM. Hierarchical model predictive control for performance enhancement of autonomous microgrids. Ain Shams Eng J 2021;12(2):1867–81. https://doi.org/10.1016/j.asej.2020.12.007.
[31] Nikam V, Kalkhambkar V. A review on control strategies for microgrids with distributed energy resources, energy storage systems, and electric vehicles. Int Trans Electr Energy Syst 2021;31(1):1–26. https://doi.org/10.1002/2050-7038.12607.
[32] Quan X, Dou X, Wu Z, Hu M, Song H, Huang AQ. A novel dominant dynamic elimination control for voltage-controlled inverter. IEEE Trans Ind Electron 2018;65(8):6800–12. https://doi.org/10.1109/TIE.2018.2805733.
[33] Shahparasti M, Mohamadian M, Yazdian A, Ahmad AA, Amini M. Derivation of a stationary-frame single-loop controller for three-phase standalone inverter supplying nonlinear loads. IEEE Trans Power Electron 2014;29(9):5063–71. https://doi.org/10.1109/TPEL.2013.2287906.
[34] Bidram A, Davoudi A. Hierarchical structure of microgrids control system. IEEE Trans Smart Grid 2012;3(4):1963–76. https://doi.org/10.1109/TSG.2012.2197425.
[35] Lu X, Guerrero JM, Sun K, Vasquez JC, Teodorescu R, Huang L. Hierarchical control of parallel AC-DC converter interfaces for hybrid microgrids. IEEE Trans Smart Grid 2014;5(2):683–92. https://doi.org/10.1109/TSG.2013.2272327.
[36] Li YW, Kao CN. An accurate power control strategy for power-electronics-interfaced distributed generation units operating in a low-voltage multibus microgrid. IEEE Trans Power Electron 2009;24(12):2977–88. https://doi.org/10.1109/TPEL.2009.2022828.
[37] Chandorkar MC, Divan DM, Adapa R. Control of parallel connected inverters in standalone ac supply systems. IEEE Trans Ind Appl 1993;29(1):136–43. https://doi.org/10.1109/28.195899.
[38] Tuladhar A, Jin H, Unger T, Mauch K. Control of parallel inverters in distributed AC power systems with consideration of line impedance effect. IEEE Trans Ind Appl 2000;36(1):131–8. https://doi.org/10.1109/28.821807.
[39] Guerrero JM, Vasquez JC, Matas J, De Vicuña LG, Castilla M. Hierarchical control of droop-controlled AC and DC microgrids - a general approach toward standardization. IEEE Trans Ind Electron 2011;58(1):158–72. https://doi.org/10.1109/TIE.2010.2066534.
[40] Liu X, Wang P, Loh PC. A hybrid AC/DC microgrid and its coordination control. IEEE Trans Smart Grid 2011;2(2):278–86. https://doi.org/10.1109/TSG.2011.2116162.
[41] Ibanez F, Mahmoud AS, Yaroslav V, Peric V, Vorobev P. Improving the power sharing transients in droop-controlled inverters with the introduction of an angle difference limiter. Int J Electr Power Energy Syst 2023;153:109371. https://doi.org/10.1016/j.ijepes.2023.109371.
[42] Rocabert J, Luna A, Blaabjerg F, Rodríguez P. Control of power converters in AC microgrids. IEEE Trans Power Electron 2012;27(11):4734–49. https://doi.org/10.1109/TPEL.2012.2199334.
[43] Wang X, Li YW, Blaabjerg F, Loh PC. Virtual-impedance-based control for voltage-source and current-source converters. IEEE Trans Power Electron 2015;30(12):7019–37. https://doi.org/10.1109/TPEL.2014.2382565.
[44] Loh PC, Newman MJ, Zmood DN, Holmes DG. A comparative analysis of multiloop voltage regulation strategies for single and three-phase UPS systems. IEEE Trans Power Electron 2003;18(5):1176–85. https://doi.org/10.1109/TPEL.2003.816199.
[45] He J, Li YW. Generalized closed-loop control schemes with embedded virtual impedances for voltage source converters with LC or LCL filters. IEEE Trans Power Electron 2012;27(4):1850–61. https://doi.org/10.1109/TPEL.2011.2168427.
[46] Blaabjerg F, Teodorescu R, Liserre M, Timbus AV. Overview of control and grid synchronization for distributed power generation systems. IEEE Trans Ind Electron 2006;53(5):1398–409. https://doi.org/10.1109/TIE.2006.881997.
[47] Coelho EAA, Cortizo PC, Garcia PFD. Small-signal stability for parallel-connected inverters in stand-alone ac supply systems. IEEE Trans Ind Appl 2002;38(2):533–42. https://doi.org/10.1109/28.993176.
[48] Ye Z, Boroyevich D, Choi JY, Lee FC. Control of circulating current in two parallel three-phase boost rectifiers. IEEE Trans Power Electron 2002;17(5):609–15. https://doi.org/10.1109/TPEL.2002.802170.
[49] Mora A, Cárdenas-Dobson R, Aguilera RP, Angulo A, Donoso F, Rodriguez J. Computationally efficient cascaded optimal switching sequence MPC for grid-connected three-level NPC converters. IEEE Trans Power Electron 2019;34(12):12464–75. https://doi.org/10.1109/TPEL.2019.2906805.
[50] Vazquez S, Marquez A, Aguilera R, Quevedo D, Leon JI, Franquelo LG. Predictive optimal switching sequence direct power control for grid-connected power converters. IEEE Trans Ind Electron 2015;62(4):2010–20. https://doi.org/10.1109/TIE.2014.2351378.
[51] Vazquez S, et al. Model predictive control for single-phase NPC converters based on optimal switching sequences. IEEE Trans Ind Electron 2016;63(12):7533–41. https://doi.org/10.1109/TIE.2016.2594227.
[52] Vazquez S, Montero C, Bordons C, Franquelo LG. Design and experimental validation of a model predictive control strategy for a VSI with long prediction horizon. In: IECON 2013-39th Annual Conference of the IEEE Industrial Electronics Society. IEEE; 2013. p. 5788–93. https://doi.org/10.1109/IECON.2013.6700083.
[53] Judewicz MG, Gonzalez SA, Echeverria NI, Fischer JR, Carrica DO. Generalized predictive current control (GPCC) for grid-tie three-phase inverters. IEEE Trans Ind Electron 2016;63(7):4475–84. https://doi.org/10.1109/TIE.2015.2508934.
[54] Mora A, et al. Model-predictive-control-based capacitor voltage balancing strategies for modular multilevel converters. IEEE Trans Ind Electron 2019;66(3):2432–43. https://doi.org/10.1109/TIE.2018.2844842.
[55] Almér S, Mariéthoz S, Morari M. Sampled data model predictive control of a voltage source inverter for reduced harmonic distortion. IEEE Trans Control Syst Technol 2013;21(5):1907–15. https://doi.org/10.1109/TCST.2012.2214777.
[56] Mariéthoz S, Morari M. Explicit model-predictive control of a PWM inverter with an LCL filter. IEEE Trans Ind Electron 2009;56(2):389–99. https://doi.org/10.1109/TIE.2008.2008793.
[57] Li Y, Grimm F, Zhang Z. Model predictive control for three-phase four-wire voltage source converters in standalone mode. In: 2019 21st European Conference on Power Electronics and Applications (EPE'19 ECCE Europe). IEEE; 2019. P-1. https://doi.org/10.23919/EPE.2019.8915479.
[58] Zhang Z, Li Z, Kazmierkowski MP, Rodriguez J, Kennel R. Robust predictive control of three-level NPC back-to-back power converter PMSG wind turbine systems with revised predictions. IEEE Trans Power Electron 2018;33(11):9588–98. https://doi.org/10.1109/TPEL.2018.2796093.
[59] Caseiro LMA, Mendes AMS, Cruz SMA. Dynamically weighted optimal switching vector model predictive control of power converters. IEEE Trans Ind Electron 2019;66(2):1235–45. https://doi.org/10.1109/TIE.2018.2829689.
[60] Harbi I, et al. Model-predictive control of multilevel inverters: challenges, recent advances, and trends. IEEE Trans Power Electron 2023;38(9):10845–68. https://doi.org/10.1109/TPEL.2023.3288499.
[61] Araujo LS, Brandao DI. Self-adaptive control for grid-forming converter with smooth transition between microgrid operating modes. Int J Electr Power Energy Syst 2022;135:107479. https://doi.org/10.1016/j.ijepes.2021.107479.
[62] Li Y, Jiang S, Cintron-Rivera JG, Peng FZ. Modeling and control of quasi-z-source inverter for distributed generation applications. IEEE Trans Ind Electron 2013;60(4):1532–41. https://doi.org/10.1109/TIE.2012.2213551.
[63] Hasanzadeh A, Onar OC, Mokhtari H, Khaligh A. A proportional-resonant controller-based wireless control strategy with a reduced number of sensors for parallel-operated UPSs. IEEE Trans Power Deliv 2010;25(1):468–78. https://doi.org/10.1109/TPWRD.2009.2034911.
[64] Komurcugil H. Rotating-sliding-line-based sliding-mode control for single-phase UPS inverters. IEEE Trans Ind Electron 2012;59(10):3719–26. https://doi.org/10.1109/TIE.2011.2159354.

[65] Zhang X, Wang Y, Yu C, Guo L, Cao R. Hysteresis model predictive control for high-power grid-connected inverters with output LCL filter. IEEE Trans Ind Electron 2016;63(1):246–56. https://doi.org/10.1109/TIE.2015.2477060.
[66] Cortés P, Ortiz G, Yuz JI, Rodríguez J, Vazquez S, Franquelo LG. Model predictive control of an inverter with output LC filter for UPS applications. IEEE Trans Ind Electron 2009;56(6):1875–83. https://doi.org/10.1109/TIE.2009.2015750.
[67] Bhatti MZA, Siddique A, Aslam W, Atiq S, Khan HS. Improved model predictive direct power control for parallel distributed generation in grid-tied microgrids. Energies 2023;16(3). https://doi.org/10.3390/en16031441.
[68] Khan HS, Kauhaniemi K. Design and FPGA-in-loop based validation of predictive hierarchical control for islanded AC microgrid. Eng Sci Technol Int J 2023;48:101557. https://doi.org/10.1016/j.jestch.2023.101557.
[69] Qi Y, Tang Y, Potti KRR, Rajashekara K. Robust power sharing control for parallel three-phase inverters against voltage measurement errors. IEEE Trans Power Electron 2020;35(12):13590–601. https://doi.org/10.1109/TPEL.2020.2993290.
[70] Zhang X, Tan L, Xian J, Zhang H, Ma Z, Kang J. Direct grid-side current model predictive control for grid-connected inverter with LCL filter. IET Power Electron 2018;11(15):2450–60. https://doi.org/10.1049/iet-pel.2018.5338.